Boundary-Layer Meteorol (2015) 154:409–426
DOI 10.1007/s10546-014-9982-7

ARTICLE

Observations of Fire–Atmosphere Interactions and Near-Surface Heat Transport on a Slope

Craig B. Clements · Daisuke Seto

Received: 22 January 2014 / Accepted: 6 November 2014 / Published online: 28 November 2014

Abstract A simple field experiment was conducted to measure and quantify fire–atmosphere interactions during a grass fire spreading up a hill under a moderate cross-slope wind. The observed fire intensity measured by passive radiometers and calculated sensible heat fluxes ranged between 90 and 120 kW m^{-2}. Observations from this experiment showed that convective heat generated from the fire front was transported downwind in the lowest 2 m and the highest plume temperatures remained in this shallow layer, suggesting the fire spread was driven primarily by the advection of near-ignition temperature gases, rather than by radiation of the tilted flame. Fire-induced circulations were present with upslope flows occurring during the fire-front passage helping to transport heat up the slope and perpendicular to the fire front. A decrease in atmospheric pressure of 0.4 hPa occurred at the fire front and coincided with a strong updraft core of nearly 8 m s^{-1}. These observations provide evidence that, even under moderately windy conditions, the pressure minimum in the fire remains rather close to the combustion zone and plume. The turbulence associated with the fire front was characterized by isotropic behaviour at 12.0 m above the ground, while less isotropic conditions were found closer to the ground due to higher horizontal variances associated with fire-induced flow at the fire front. From analysis of the turbulence kinetic energy budget terms, it was found that buoyancy production, rather than shear generation, had a larger contribution to the generation of turbulence kinetic energy, even during a highly sheared and moderate ambient wind.

Keywords Fire–atmosphere interactions · Fire behaviour · Fire weather · Sloping terrain · Turbulence · Wildfire

C. B. Clements (✉) · D. Seto
Fire Weather Research Laboratory, Department of Meteorology and Climate Science,
San José State University, One Washington Square, DH 620, San Jose, CA 95192, USA
e-mail: craig.clements@sjsu.edu

1 Introduction

Wildland fire radically modifies the atmospheric surface layer by emitting sensible, latent, and radiant heat fluxes that affect the ambient meteorological fields downwind of and surrounding the fire front. When the heat supplied by a fire is sufficient enough to overcome the kinetic energy of the ambient flow, the atmosphere becomes coupled to the fire (Byram 1959; Clark et al. 1996). The coupling of the atmosphere to the fire directly influences fire behaviour by the generation of fire-induced winds that can further drive the fire spread (Sun et al. 2009), and in some cases in directions that are opposite to the ambient wind direction.

Wildland fire in regions of complex terrain is often associated with extreme fire behaviour (Sharples 2009). Extreme fire behaviour implies a level of fire behaviour characteristics that would make a fire difficult to control and can result in compromised fire fighter safety and increased danger to communities. It can be summarized in a more formal definition following Werth et al. (2011) as "fire spread other than steady surface spread, especially when it involves rapid increases." Kochanski et al. (2013) demonstrated that the development of extreme or erratic fire behaviour may depend on the structure of the low-level vertical shear in the upstream ambient wind field. Many occurrences of extreme fire behaviour are caused by the interaction of the fire front and the local wind systems found in mountainous terrain (Clements 2011). Typically, wind direction changes twice daily within mountain valleys (Whiteman 2000), and is accompanied by changes in atmospheric stability as the valley atmosphere undergoes transition from stable conditions with down-valley flow to unstable conditions with up-valley flow. This transition can lead to vertical wind shear that is often present near the surface affecting the fire behaviour (Clements 2011). Extreme fire behaviour in valleys also occurs when there is an interaction between the along-valley flow and other mesoscale circulations such as the sea breeze (Cunningham 2007). Such interactions have led to the development of fire whirls associated with vertical shear induced by the two opposing flows (Seto and Clements 2011).

Over sloping terrain, the ambient wind is thought to have an effect on the rate of fire spread comparable to the slope angle (Weise and Biging 1997). Often, fires 'blow-up' as they accelerate upslope (Viegas 2005), where blow-up is defined as a fire that increases its fire-line intensity or rate of spread suddenly (Potter 2012). This phenomenon has been observed on steep slopes and in canyons, both in the field (Viegas 2005) and during laboratory experiments (Viegas 2005; Viegas and Simeoni 2010; Dupuy and Maréchal 2011; Pimont et al. 2012). The increase in spread rate is caused by the fire's increased contact with the fuels since the fuels are closer in proximity to the fire due to the higher elevation of the fuel bed relative to the flame front. There also is an absence of the inflow on the direct uphill side of the fire front, as is illustrated in studies of trench fires (Sharples et al. 2010) where the fire is surrounded by fuels on three sides and by the atmosphere on one. Additionally, the flow can accelerate uphill (Taylor and Teunissen 1987; Moreira and Santos 2012) promoting the increase in fire-line intensity and the rate of fire spread (Kochanski et al. 2009). One of the most extensive studies on fire behaviour in canyons was that of Viegas and Pita (2004) who carried out a series of burning experiments in the laboratory investigating canyon geometry including closed canyon topography and various slope angles. Their results were compared to a canyon fire as part of the Gestosa field experiments conducted in central Portugal in 2001 (Viegas et al. 2002). Results from these experiments suggest that fire blow-up occurs even in shallow canyons without any ambient flow over the fire.

While there has been an increase in studies focusing on fire-atmospheric interactions, most have been conducted using coupled fire–atmosphere numerical models (Coen 2005; Mell et al. 2007; Linn et al. 2010; Kochanski et al. 2013; Coen et al. 2013; Filippi et al. 2013)

and few have focused on observations from field campaigns. The more comprehensive field studies have been made over flat terrain with homogenous fuels (i.e., Cheney et al. 1998; Clements et al. 2007). Therefore, to better understand fire behaviour in complex terrain and to study the role of fire–atmosphere interactions over slopes, a simple field experiment was conducted. The goal of this study is to quantify the meteorological properties of the near-surface environment during a fire-front passage (FFP) over a slope and to determine the influence of fire–atmosphere interactions on heat transport and fire spread. Fire-front passage is typically associated with sharp changes in the near-surface environment including increased surface winds at the fire front, isolated updrafts, a sharp increase in air temperature, an increase in turbulent kinetic energy, and at times, downdrafts behind the fire front (Clements et al. 2008).

While this study quantifies unique fire–atmosphere interactions over hilly terrain, there are limitations that need to be acknowledged. Mainly, the fire behaviour and fuel properties were not adequately quantified and this limits the analysis of fire behaviour and the influence the atmosphere has on its evolution. However, the data presented here show unique features of the fire–atmosphere system that can be useful for the evaluation of coupled fire–atmosphere numerical modelling systems for cases of simple slopes.

2 Experimental Design

The experimental design was coordinated with an annual firefighter training exercise conducted at the Parks Reserve Forces Training Area, historically known as Camp Parks, located in Dublin, California (Fig. 1). The measurement campaign took place on 24 June 2010 on a hillside with grass as the main fuel type. The goal was to take advantage of fires ignited for suppression training and this provided a rare opportunity to measure meteorological conditions during a grass fire that was allowed to spread freely upslope as a head fire.

2.1 Site Characteristics

The experimental site (121°52′ 26.39″W, 37°43′ 50.81″N) is surrounded by housing developments to the north and east and the city of Dublin to the south and west (Fig. 1). Small hills and knolls with intervening shallow valleys characterize the area's physical geography. The terrain relief is approximately 50–150 m in height at an elevation of 150 m above mean sea level. California annual grassland is the dominant plant community at the site and is composed of native and non-native annual and perennial grasses interspersed with species of native and non-native forbs (a herbaceous flowering plant) that were nearly fully cured (Fig. 2). Common grasses include soft chess, wild oat, ripgut brome, and Italian ryegrass. Forbs that are found within this community include yellow-star thistle, fiddleneck, California poppy, field bindweed, arrowleaf balsamroot, and Ithuriel's spear (http://www.parks.army.mil). There were also areas within the burn plot that consisted of dense patches of 2–2.5 m tall wild mustard. The slope angle of the plot was 20°. Fuel loadings were sampled within the burn plot (Fig. 1), but the samples were contaminated during transport. Consequently, we estimate the fuel loadings at 0.12 kg m^{-2} according to similar fuel conditions in the region (Seto and Clements 2011).

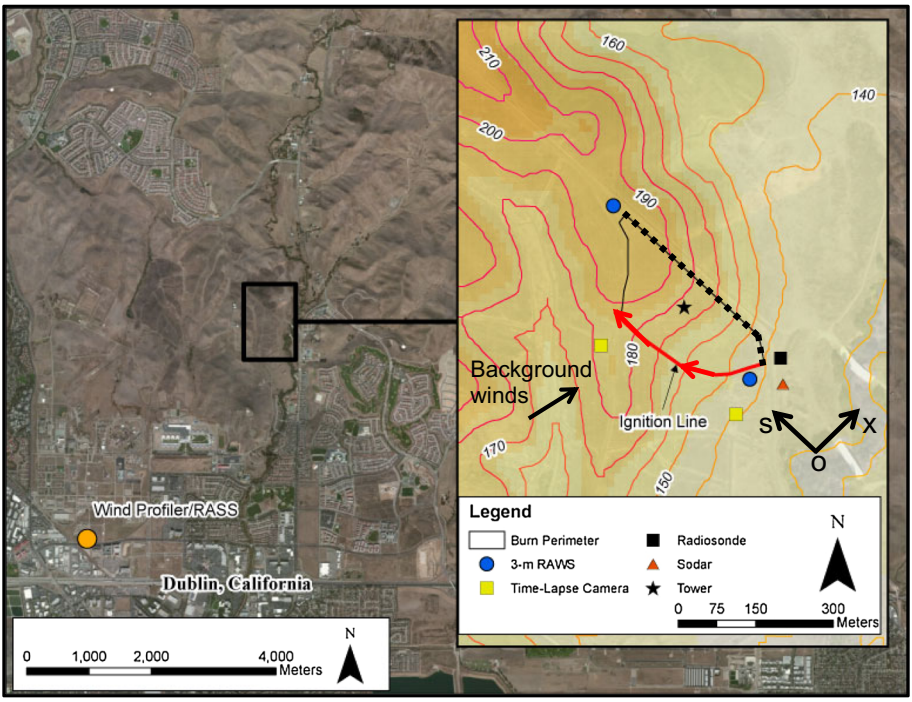

Fig. 1 Aerial photograph of the experimental site showing regional features, and an *inset* topographic map showing instrument locations and fire perimeter. The *ignition line* is indicated by a *red line* with *arrows* pointing in the direction of ignition. The backing fire, along the eastern fire perimeter, is indicated by the *dashed line*

Fig. 2 Photograph of burn plot showing measurement tower, marking poles, and fuel structure. View is directed up the slope from the south-east

Table 1 Summary of the instrumentation used on the interior tower

Instrument (manufacturer, model)	Sampling rate (Hz)	Sensor height (m a.g.l.)	Notes
3-D sonic anemometer	10	12	Custom-calibrated above 110 °C
(Applied Technology Inc., SATI Sx)			
3d propeller anemometer	1	12	
(R.M. Young Company, 27005)		1.9	
Type E Thermocouple	5	1, 2, 3, . . . 10	0.076 mm diameter at bead
(Omega Inc., 5SC-TT-E-40-36)			
Total heat flux sensor	10	0.6	180° field of view
(Hukseflux, SBG01)			<250 ms response time
Radiative heat flux sensor	10	0.6	150° field of view
(Medtherm Corp., 64P-50-24)			<100 ms response time
Barometric pressure sensor	1	2.1	0.025 hPa resolution
(R.M. Young Company, 61302V)			1.8 Hz update rate

2.2 Instrumentation and Experimental Layout

The experiment was designed to measure near-surface meteorological variables during fire-front passage along a uniform slope. The main observational platform was a 12-m steel tower erected in the middle of the slope (Fig. 2), with the tower instrumented at multiple heights with sensors to measure winds and temperature (Table 1). All instruments were sampled using a Campbell Scientific, Inc. (CSI), CR3000 data logger. Wind speeds were measured at 12.0 m above ground level (a.g.l.) using a 3-D sonic anemometer (Applied Technologies, Inc., SATI Sx style probe) and a collocated Gill UVW propellor anemometer (R.M. Young 27005). The sonic anemometer was sampled at 10 Hz while the propellor anemometer was sampled at 1 Hz. An additional UVW propellor anemometer was mounted at 1.9 m a.g.l. to measure winds near the flame front. The horizontal wind velocity components were rotated into streamwise and crosswise u and v, respectively, and the vertical velocity w was tilt-corrected following Wilczak et al. (2001).

A fine-wire thermocouple array (Omega Engineering, Inc., model 5SC-TT-E-40-36) was installed on the tower with thermocouples mounted at 1-m vertical spacing, and sampled at a frequency of 5 Hz. The array allowed the vertical thermal structure of the fire plume to be measured at a high temporal scale. Surface pressure was sampled at 2.1 m a.g.l. using a R.M. Young barometer (model 62302V), with a pressure port (R.M. Young, model 61002) attached to the inlet port of the barometer to eliminate the flow effects on the pressure measurement. In addition to the meteorological measurements, fire-front heat fluxes were measured at 0.6 m a.g.l. using a Schmidt–Boelter gauge total heat-flux sensor (Hukseflux, SBG01) and a Gardon gauge radiative heat-flux sensor (Medtherm, 64P-50-24) equipped with a sapphire window. Both sensors were water-cooled using a small DC powered pump and reservoir mounted in an enclosure. The sensors were pointing at 161° across and down the slope and located approximately 2 m downslope from the tower base.

Two portable weather stations were also installed at the site, one at the top of the slope and one at the bottom. Temperature and humidity were measured using a CSI CS215 probe, and wind speed and direction were measured using a R.M. Young 5103 propeller anemometer. The sensors were sampled at 1 Hz using a CSI CR1000 datalogger, and data were averaged

and stored at 1-min intervals. Also located at the bottom of the slope was the Doppler sodar (Atmospheric Systems, Corp., model ASC-4000) that measured vertical profiles of horizontal and vertical wind speeds up to 200 m a.g.l. averaged at 5-min intervals. A radar wind profiler and radio acoustic sounding system (RASS) managed by the Bay Area Air Pollution Management District and located approximately 4 km south-west of the site operated throughout the experimental period (Fig. 1). The profiler provided wind profiles up to 1.5 km a.g.l. and temperature profiles up to 1 km a.g.l. Additionally, an upper air sounding (GRAW Radiosondes GmbH & Co. KG., DFM-06) was made at the time of ignition.

Two camera systems were used to document the fire front and plume behaviour including a digital video camera and a digital single-lens reflex camera for time-lapse photography, with the latter camera located on the ridge to the west of the burn block and the video camera located at the base of the slope (Fig. 1). To help facilitate fire behaviour measurements and photogrammetric analysis, markers were placed on 3-m poles every 10 m in a line running up the slope (Fig. 2), however, due to the change in expected wind direction that occurred on the day of the experiment, the markers were of minimal use in our analysis.

2.3 Ignition Strategy

The ignition pattern was designed to allow for a free burning head fire (a fire that burns freely with the wind and/or slope) to burn up the slope, through the instrument tower and marker array. In order to isolate processes related to the interaction of the fire front and the near-surface flow, it was planned that only a simple head fire would be ignited and that no backing fire (a fire that burns against the wind in a more controlled manner) would be ignited. Typically, backing fires are used by fire management agencies for vegetation management because they are lower intensity and easier to control. Because the weather conditions during the day of the burn were less than ideal with higher wind speeds than expected, the decision was made to use a backing fire along the eastern perimeter of the burn unit (Fig. 1). The ignition team ignited the burn plot on its most eastern boundary starting at the top of the slope and working their way down to the bottom (indicated by dashed line in Fig. 1). From that point the ignition team separated into three groups staggered and separated by a few metres as they walked along the base of the slope towards the west, finishing the ignition by looping around to just west of where they started, but on the opposite side of the burn unit.

3 Results and Discussion

3.1 Ambient Meteorological Conditions

The conditions on the day of the experiment (24 June 2010) were not ideal; during ignition at 0939 Pacific Daylight Time (PDT) the wind speed was much higher than anticipated at nearly 9 m s^{-1} at the hilltop and 3 m s^{-1} at the bottom (Fig. 3). The wind direction associated with these stronger surface winds was not desirable, coming across the slope (i.e., cross-slope flow) where the ignition was set at the bottom of the slope. Compared to the previous day, the relative humidity and air temperature were also higher at 80 % and 12 °C, respectively. At 0805 PDT on the morning of the burn, eight fuel moisture samples of fine dead fuels were collected near the tower base. The fine dead fuel moisture content (fuel particles <6 mm in diameter) averaged 42.5 %, which is considered high, but given the high humidity, these

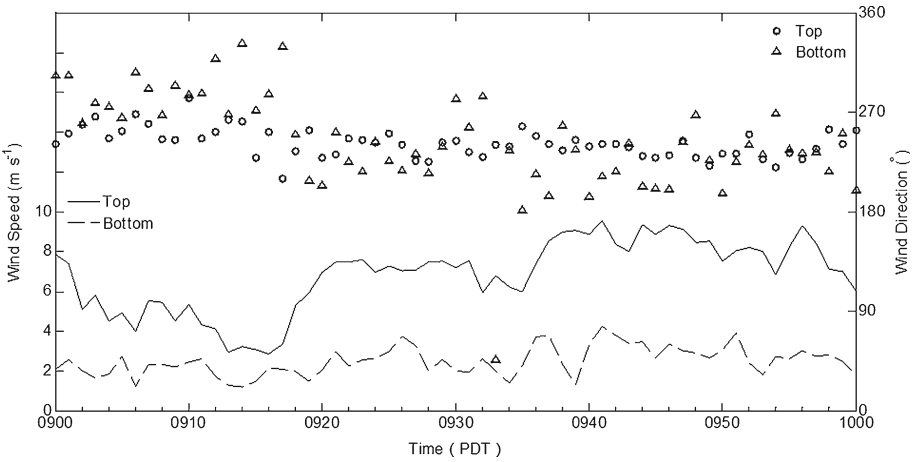

Fig. 3 Time series of wind speed (*line*) and direction (*symbols*) from the two portable weather stations located at the top and bottom of the hill

values are reasonable. Fuel moisture was also collected on the previous day, 23 June 2010, and ranged between 10–25 % due to the drier daytime conditions.

Even though conditions were not ideal, advantage was taken of the opportunity to monitor fire–atmosphere interactions under such conditions, which to our knowledge has not been accomplished before; in particular, fire behaviour on a slope with strong cross-slope flow. Observations from the radar wind profiler (Fig. 4) show that the ambient winds above the surface ranged from west-south-westerly and west-north-westerly with a nearly constant speed with height after 0900 PDT. However, the sounding taken at the bottom of the slope near the ignition line shows that strong vertical wind shear was present in the lowest 500 m a.g.l. (Fig. 5b). The sounding also shows that a shallow superadiabatic layer was present in the lowest 40 m a.g.l., while up to 250 m a.g.l., the potential temperature profile was stable (Fig. 5a). A stronger stable layer was present between 250 m and 300 m a.g.l., and above this layer the profile remained stable up to a capping inversion at 500 m a.g.l. The deep stable layer and increased water vapour mixing ratios within the lowest 500 m a.g.l. indicate the presence of a marine boundary layer over the region.

3.2 Plume Evolution

The evolution of the smoke plume and fire front was monitored using both time-lapse still photography and digital video. The camera positions are indicated in Fig. 1. Figure 6 shows a suite of time-lapse photos for various times throughout the firing operations. At 0933:28 PDT (Fig. 6a), the plume from the back-burning operations along the eastern boundary is visible. At the bottom of the slope the plume is more developed, as this is the time when the ignition crews conducted ignitions along the southern boundary of the plot (Fig. 1; red solid line). Smoke is initially to be transported in an upslope direction, which was first observed at 0935:59 PDT (Fig. 6b) and during the development of the smoke column. Surface winds at the base of the slope (Fig. 3) switched briefly to north-easterly at this time and indicate the relative influence of the fire on the surface winds. The influence of the fire and plume is even more dramatically illustrated by the vertical wind profiles obtained by the sodar located at the slope bottom (Fig. 7). At 0935 PDT there is a distinct wind reversal

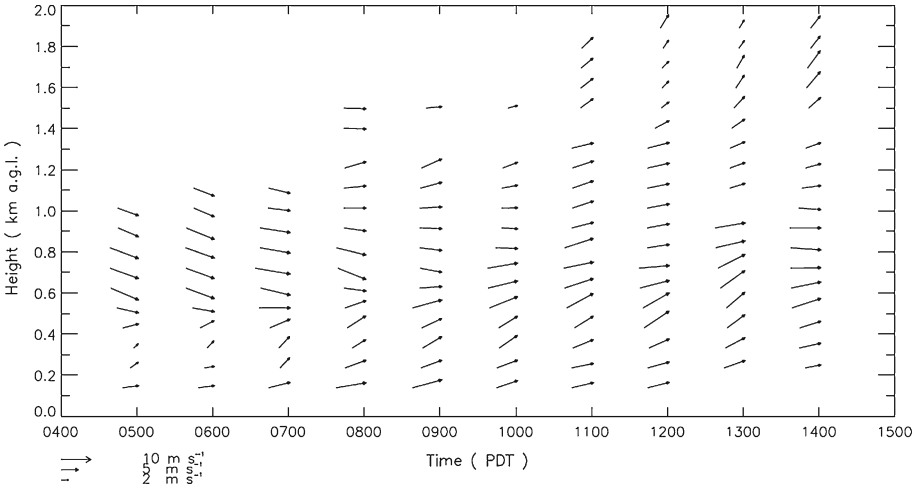

Fig. 4 Time-height plot of winds taken from the radar wind profiler located south-west of the experimental plot

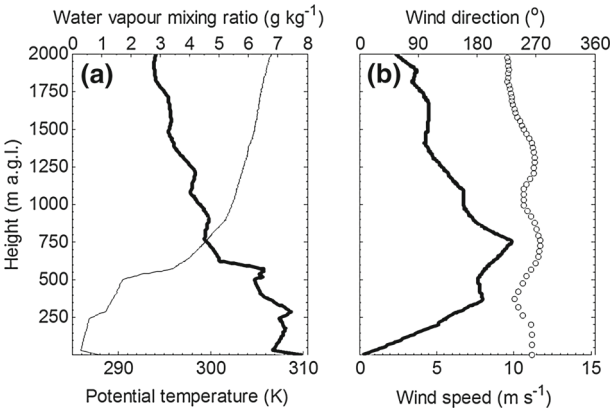

Fig. 5 Profiles of **a** potential temperature (*thin line*) and water vapour mixing ratio (*thick line*), and **b** wind speed (*line*) and direction (*symbols*) taken from a rawinsonde sounding made just before ignition on 24 June 2010 at 0916:32 PDT

aloft between 150 and 220 m a.g.l., likely produced in response to thermal instabilities generated by the plume. This observed reversal is very intermittent and does not occur again even as the plume and fire intensity strengthen throughout the burning operations (Fig. 6e, f).

At 0942:14 PDT strong inflow along the surface is observed by the smoke moving from the bottom and southern side of the slope into the base of the smoke column (red arrow, Fig. 6g). This southerly flow indicates fire-induced winds developed in response to the instabilities produced by the heat release from the fire front even though a strong cross-slope flow was present at the hilltop (Fig. 3). This near-surface entrainment continues as the ignition line and fire front are established higher up the slope. Also during this time, the developed smoke column was bent over (Fig. 6h–k) and rotating in the clockwise direction.

Fig. 6 Time-lapse photographs showing ignition procedure and plume evolution. Times are PDT and indicated in each panel. The *small red arrow* in **g** shows the entrainment indraft direction. Orientation of plot and reference axis from Fig. 1 is shown in (**a**). The smoke column started rotating in a clockwise direction after 0940:36 (**e**)

The fire-front passage at the tower occurred at 0942:30 PDT (Fig. 6h), however the exact time of fire-front passage is difficult to discern from the photographs. A more precise estimate is made from thermodynamic data discussed in Sect. 3.3. Also difficult to determine from the photo series are the fire behaviour characteristics such as flame height, flame length, rate of spread, and fire-front geometry. This is partly due to the camera position, but also the firing pattern used for ignition. As discussed previously, in order to have the fire front spread through the tower, the fire line was set using multiple staggered ignition lines. This caused the fire front to have a complex, multiple-line, flanking structure rather than a simple single-line fire. As the ignition team moved to the western edge of the burn block (Fig. 6j–l), the fire front had a more characteristic shape of a single head fire, but this is hard to discern from the photographs.

3.3 Near-Surface Thermodynamic Structure and Heat Transport

The thermodynamic structure of the near-surface environment during the fire-front passage was analyzed using in situ measurements made on the tower and at the ground. Figure 8 shows the plume temperature measured using fine-wire thermocouples mounted on the tower and total and radiant heat fluxes measured near the tower base. The sensors were pointed nearly

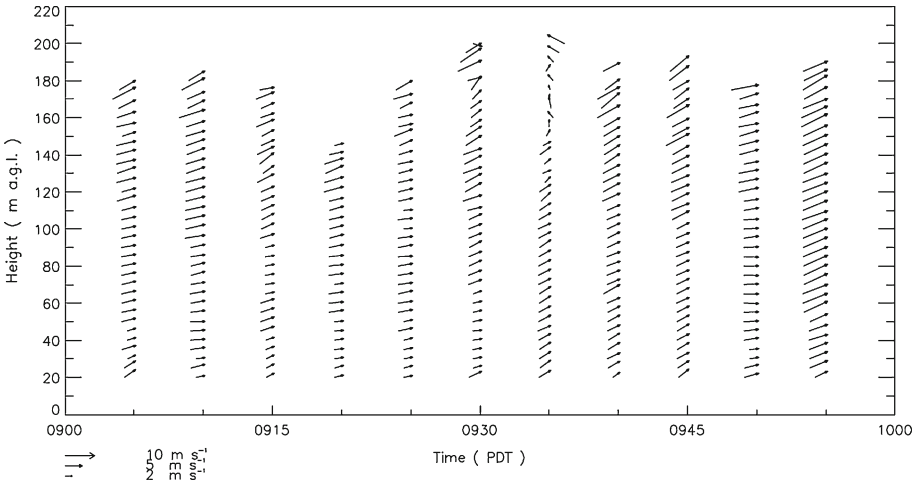

Fig. 7 Time-height plot of 5-min averaged vertical wind profiles measured by sodar

horizontal towards the approaching fire front. While the tower measurements do not extend through the entire plume, they do provide high spatial and temporal resolution observations of temperature and heat flux in the lowest 12 m near the surface. As the plume advected past the tower, warm air advection occurred at all levels ahead of the fire-front arrival with the highest air temperatures near the surface. At 0942:10 PDT, an initial plume passage with temperatures of nearly 100 °C occurred followed for a few seconds by cooler ambient air before the blast of heat associated with the main fire front arrival at 0942:30 PDT. At this time, the maximum air temperature of nearly 350 °C was observed within the lowest 2 m a.g.l. The hottest portion of the plume remains at the surface advecting downwind of the fire front, and is associated with strong flow with speeds of 7 m s^{-1} (Fig. 3). Furthermore, increases in both the total and radiant heat fluxes are shown to correspond well with high plume temperatures (Fig. 8). For example, at 0942:17 PDT the total heat flux, Q_{total}, increased to 120 kW m^{-2} just before the plume passes the tower as indicated by the increase in temperature between the surface and 5 m a.g.l. The radiant heat flux, Q_{rad}, peaks at 55 kW m^{-2}, about half of the total heat flux. Because the heat-flux sensors were located 2 m from the tower, the peaks in heat flux do not necessarily correspond with all peaks in plume temperature. However, at 0942:35 PDT, the Q_{total} of 90 kW m^{-2} corresponds well with a significant plume passage indicated by an increase in temperature from near surface to 5 m a.g.l. (Fig. 8).

3.4 Fire-Induced Circulations

The kinematic structure of the tilted convective smoke column (Fig. 6) is associated with a clockwise rotation and oriented along the ambient mean flow (OX axis in Fig. 1) as a single longitudinal vortex (Forethofer and Goodrick 2011). To illustrate the airflow in and around the passing fire front at the surface, the magnitude of the vectors $V(u, v)$ is presented in Fig. 9. The vector $V(u, v)$ was in the cross-slope direction at both 12.0 m and 1.9 m a.g.l. until 0941:30 PDT. Ahead of the approaching fire front, a sustained period of downslope flow first developed at 1.9 m a.g.l. between 0941:40 and 0942:10 PDT while the flow at 12.0 m a.g.l. was upslope. A sudden shift from downslope to upslope flow with increased velocities occurred at 0942:20 PDT at 1.9 m a.g.l. indicating a horizontal directional shear

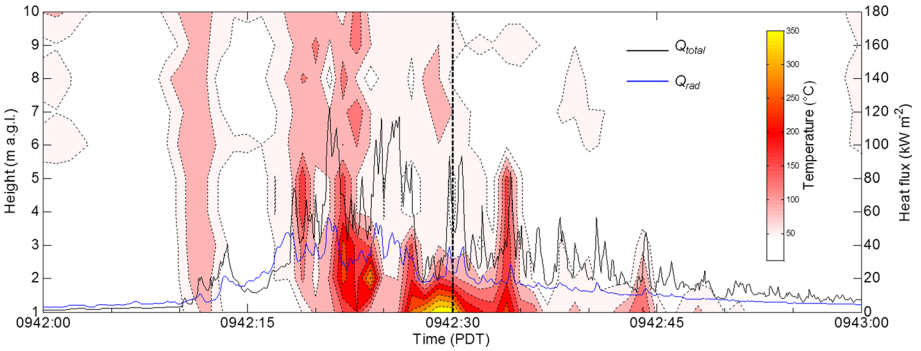

Fig. 8 Composite plot showing time-height analysis of shaded contours of 1-s near-surface temperature overlain with time series of total (*black line*) and radiant heat (*blue line*) fluxes. *Black dashed line* indicates time of fire-front passage

environment (Fig. 9b). It is plausible that the interaction of cross-slope flow and fire-induced downslope and upslope flows generated the low-level horizontal shear without influence from the background ambient wind shear. As soon as the fire front passed the tower, the propellor anemometer at 1.9 m a.g.l. was damaged by fire with no operation after 0942:30 PDT, while at 12.0 m a.g.l., upslope flow continued behind the fire front. The complex flows around the fire front may have affected the direction of fire spread; the observed fire- and terrain-induced upslope component of the flow supports the concept of fire-line rotation and multidirectional spread on a slope as described by Viegas (2002, 2004). Unfortunately, these types of fire behaviour cannot be confirmed herein due to the lack of observations of fire-front geometry.

Observations from the tower do suggest the relative importance of near-surface advection and its effect on heat transport and the preheating of fuels. Comparing our results to the laboratory studies of Dupuy and Maréchal (2011) further indicates that, in our case, convection may be more important than radiation for the duration of the fire-front passage. Dupuy and Maréchal (2011) show that, close to the fireline, radiative heating is the dominant heat transfer mechanism on slopes between 0° and 20°. Convective heating was also found to be significant, becoming one-third of the total heat flux on their 20° slope. Our measurements show that ahead of the approaching fire front, a sustained period of downslope flow occurred near the surface between 0941:40 and 0942:20 PDT (Fig. 9). This flow transported the near-

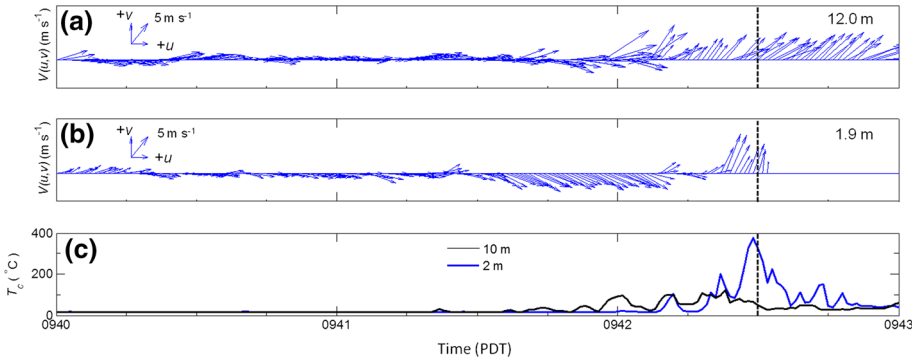

Fig. 9 Time series of the horizontal vector $V(u, v)$ at **a** 12.0 m, **b** 1.9 m, and **c** thermocouple temperatures T_c measured at the tower. *Black dashed line* indicates time of fire-front passage

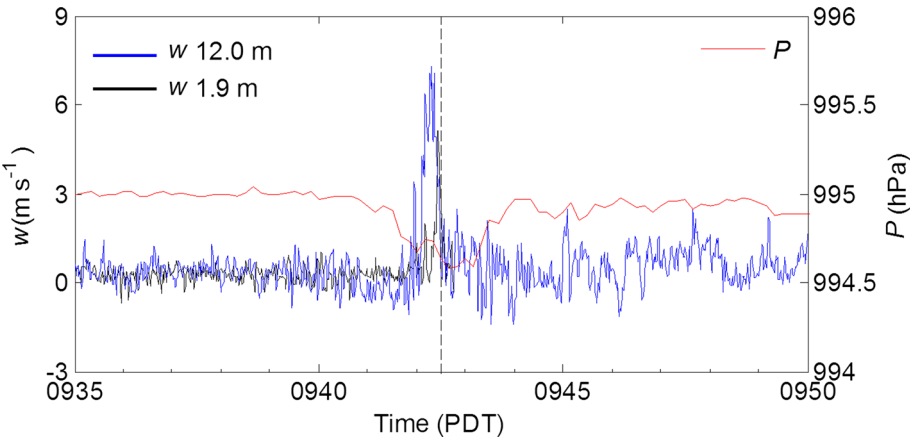

Fig. 10 Time series of atmospheric pressure P and vertical velocities w measured at the tower. *Black dashed line* indicates time of fire-front passage

surface plume downslope resulting in a decrease in total incident heat flux while the radiative heat flux remained higher ahead of the fire front (Fig. 8). The sudden shift from downslope to upslope flow, observed near the surface after 0942:20 PDT (Fig. 9b), was accompanied with higher air temperatures above 300 °C (Fig. 8). This observation suggests that fire spread is driven primarily by the advection of high, near-ignition temperature gases, rather than by radiation of the tilted flame. Our results are in agreement with Dupuy and Maréchal for the pre fire-front regime and also with Morandini and Silvani (2010) who showed that mixed radiant-convective heat transfer promotes preheating of the unburned fuel in an environment where fire spread is driven by wind.

Further analysis of the flow during the fire-front passage shows that a minimum in atmospheric pressure coincided with a strong updraft core of 8 m s^{-1} (Fig. 10). The ambient atmospheric pressure ranged between 994.9 and 995 hPa before the fire-front passage, and the first pressure decrease to 994.8 hPa occurred at 09:41:30 PDT when the plume passed the upper part of the tower (Figs. 9c, 10). The lowest pressure of 994.6 hPa, a decrease of 0.4 hPa, occurred when the fire passed the tower. This observation provides evidence that, even under moderately windy conditions, the pressure minimum of the fire remains rather close to the combustion zone, and even after the fire-front passage the pressure remained below the ambient level for nearly 20 s. Our measurements contradict the study of Clark et al. (1996) who described the low pressure zone as an area of convergence and proposed that when ambient winds are strong the convergence zone is located downwind of the fire front. Our observations indicate that the region of the pressure minimum remains close to the fire front and that the pressure minimum may be responsible for the observed acceleration of horizontal flows into the fire, since the pressure minimum remains rather close to the combustion zone and plume.

In contrast to other studies (e.g., Clements et al. 2007), downdrafts were not observed behind the fire front. However, downdrafts just ahead of the fire front at 12 m a.g.l. were present in the 10-Hz sonic anemometer data (not shown). We speculate that any downdrafts that do develop behind the fire front are likely entrained into the rotating smoke column or simply that the measurement tower did not capture these flows because of the location of the tower relative to the fire front.

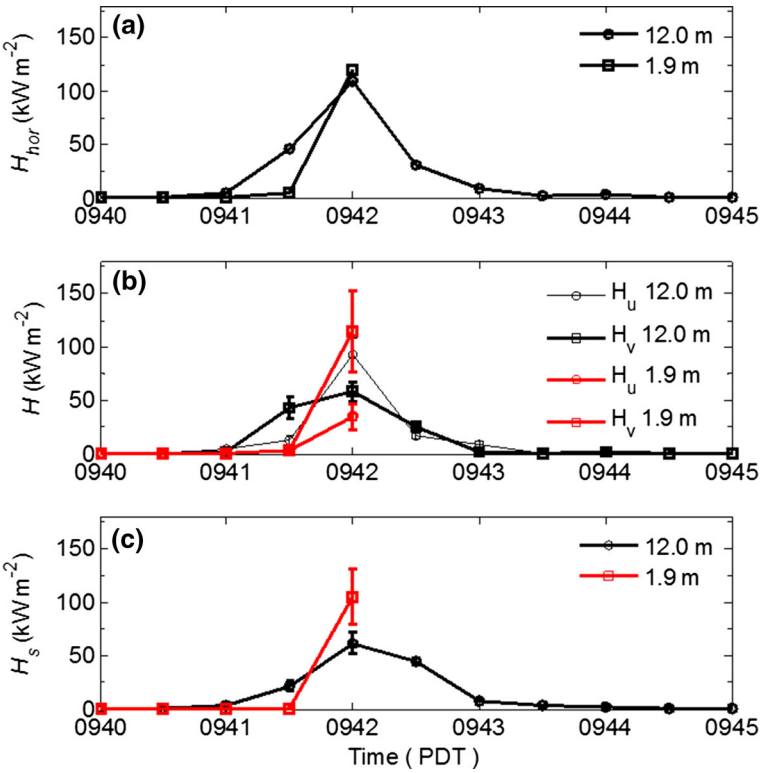

Fig. 11 Time series of **a** the horizontal sensible heat fluxes from Eq. 1 measured at 12.0 and 1.9 m; **b** streamwise (H_u) and crosswise (H_v) heat fluxes measured at 12.0 m (*black*) and 1.9 m a.g.l. (*red*); **c** vertical sensible heat fluxes. *Error bars* denote ±1 standard error. Missing data at 1.9 m AGL level due to instrument damage caused by fire after the fire-front passage

3.5 Turbulence Statistics

To further assess the role of near-surface heat transport along the slope, horizontal and vertical components of the turbulent sensible heat flux were compared, with sensible heat fluxes calculated using eddy covariance. The vertical sensible heat flux is $H_s = \overline{\rho} c_p \overline{w'T'}$, where $\overline{\rho}$ is the average density of air (1.2 kg m^{-3}), assumed to be constant, c_p is the heat capacity of air (1,004 J kg^{-1} K^{-1}), w' is the perturbation vertical velocity, and T' is the perturbation temperature. The overbar represents a Reynolds average of 30 s while perturbations were calculated by subtracting the instantaneous values from the 15-min mean. The horizontal heat flux is given by

$$H_{\text{hor}} = \overline{\rho} c_p \left[\left(\overline{u'T'} \right)^2 + \left(\overline{v'T'} \right)^2 \right]^{1/2}, \quad (1)$$

where u' and v' are the perturbation velocities in the streamwise and crosswise components, respectively. The turbulent heat fluxes were calculated using 10-Hz sonic velocity components and temperature for the 12.0-m level, whereas 1-Hz thermocouple temperatures at 2 m a.g.l. and propellor anemometer velocities at 1.9 m a.g.l. were used for the 1.9-m level.

Figure 11 shows the time series of horizontal heat flux during the fire-front passage calculated from Eq. 1. The greatest heat transport occurred at the lowest level near the

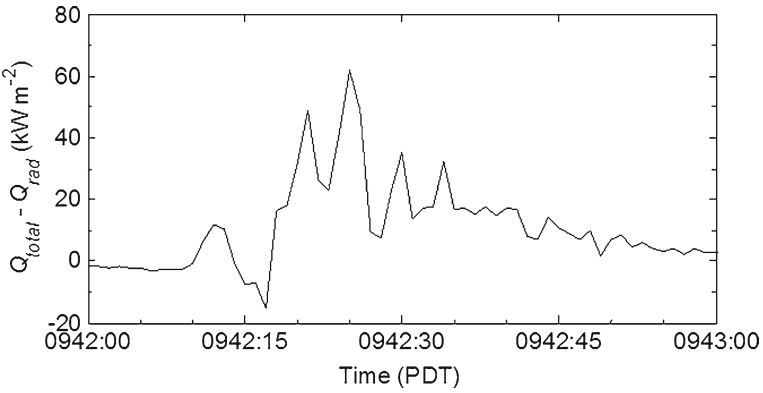

Fig. 12 Time series of Q_{total}–Q_{rad} during the fire-front passage

surface. The total horizontal sensible heat flux at 1.9 m a.g.l. reached a maximum of 120 kW m^{-2} during the fire-front passage (0942:00 PDT), most of which was associated with the along-slope component, $\overline{v'T'}$ (115 kW m^{-2}). At 12.0 m a.g.l., the greatest heat flux was in the streamwise direction, $\overline{u'T'} \approx 93\,\text{kW m}^{-2}$, while in the along-slope direction, $H_{\text{hor}} = 58\,\text{kW m}^{-2}$. These magnitudes are similar to the horizontal convective heat fluxes measured from the heat-flux radiometers as the difference between Q_{total} and Q_{rad}, ≈18–55 kW m^{-2} (Fig. 12). A comparison between the horizontal and vertical sensible heat fluxes shows that the vertical heat flux ($H_{\text{s}} = 62\,\text{kW m}^{-2}$) at 12.0 m a.g.l. is almost half of the horizontal heat flux ($H_{\text{hor}} = 109\,\text{kW m}^{-2}$), but near the surface, the heat fluxes are nearly equal, $H_{\text{s}} = 106\,\text{kW m}^{-2}$ and $H_{\text{hor}} = 120\,\text{kW m}^{-2}$. These observations indicate that, in this case, the strongest heating occurs at the surface, not in the along-wind direction, but rather in the upslope direction even with the mean flow across the slope. As the fire front was driven across the slope, fire-induced circulations developed (Fig. 9a) and transported most of the heat upslope at the surface while at 12.0 m a.g.l. heat was transported within the plume in the along-wind direction.

The ambient turbulence regime of the surface layer surrounding a fire is dominated by both the fuel and terrain roughness characteristics. The fire itself also generates turbulence structures that are associated with the buoyancy of the fire front and resulting plume, and fire-induced circulations that create strong near-surface vertical wind shear (Clements et al. 2008; Seto et al. 2013). To characterize the fire-induced turbulence associated with fire front passage, the average turbulence kinetic energy (TKE), $\bar{e} = 0.5\left(\sigma_u^2 + \sigma_v^2 + \sigma_w^2\right)$ was calculated. The velocity variances, σ_i, measured in the smoke plume at $z = 12.0$ m a.g.l. (Fig. 13a) indicate that both horizontal and vertical velocity variances increased when the smoke plume passed the tower between 0941:30 and 0942:30 PDT (Fig. 12a). The in-plume variance ratios σ_u^2/σ_w^2 and σ_v^2/σ_w^2 approached a value of 1 at 0942 PDT similar to observations by Clements et al. (2008) during a wind-driven grass fire over flat terrain and suggests near-isotropic turbulence behaviour in the plume. At $z = 1.9$ m a.g.l. during the fire front passage, both σ_u and σ_v are dominant over σ_w indicating less isotropy at the surface and larger TKE ($\bar{e} \approx 14\,\text{m}^2\,\text{s}^{-2}$) within the smoke plume at 12.0 m a.g.l. However, our 1-Hz sampling rate made at 1.9 m a.g.l. does not provide sufficient temporal resolution, and thus the TKE near the surface is likely higher than our measured values.

To assess the role of shear and buoyancy on TKE generation, terms in the TKE budget equation are estimated from the tower data. Assuming horizontal homogeneity and neglecting subsidence, the TKE budget equation (Stull 1988) is expressed as

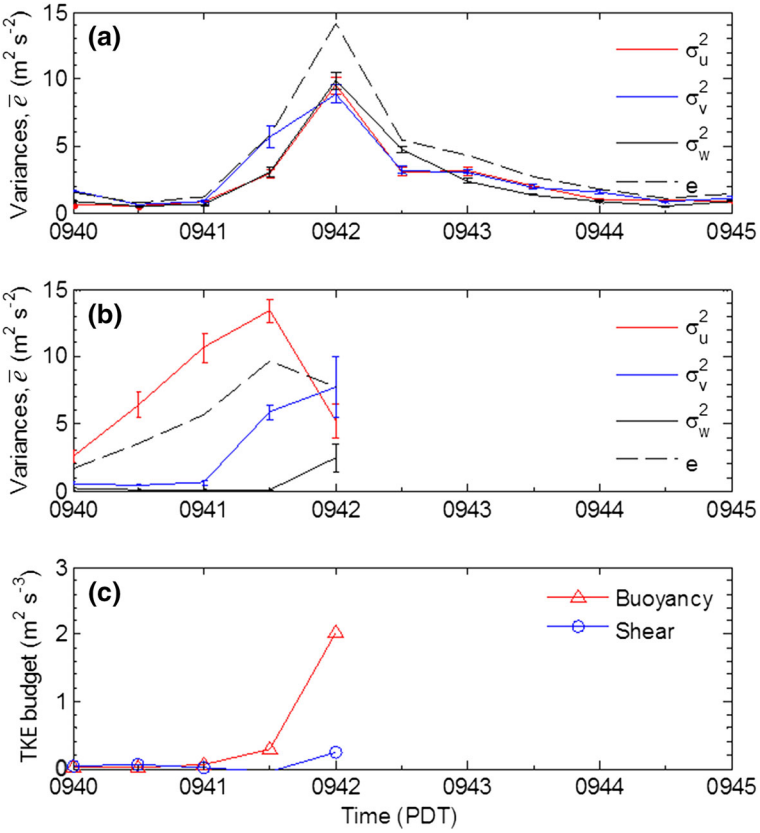

Fig. 13 Time series of velocity variances and TKE ($\overline{e}$) measured at **a** 12.0 m a.g.l., **b** 1.9 m a.g.l., and **c** buoyancy production and shear generation terms in the TKE tendency equation. *Error bars* denote ±1 standard error. Missing data at 1.9 m a.g.l. level due to instrument damage caused by fire after fire-front passage

$$\frac{\partial \overline{e}}{\partial t} = \frac{g}{T_v}\overline{w'T_v'} - \overline{u'w'}\frac{\partial \overline{U}}{\partial z} - \frac{\partial \overline{w'e}}{\partial z} - \frac{1}{\overline{\rho}}\frac{\partial\left(\overline{w'p'}\right)}{\partial z} - \varepsilon, \tag{2}$$

where the first term on the right-hand side of the equation is the buoyancy production and the second term is the shear production. These two terms are of particular interest and therefore we evaluate the relative importance of each term using the wind velocities and temperature measured at heights of 1.9 and 12.0 m. The last three terms, turbulence transport, pressure correlation, and the dissipation, are not estimated because we do not have adequate measurements to evaluate these. The heat flux in the buoyancy production term and the momentum flux in the shear generation term are obtained from layer-averaged values.

Despite the moderate winds on the day of the burn, the buoyancy production (Fig. 13c) increased during fire-front passage due to a large increase in the sensible heat flux, $\overline{w'T_v'}$. The buoyancy production is larger in magnitude than the shear generation indicating that the production of turbulence is characteristic of free convection near and above the fire front. It is plausible that under weaker ambient winds fire-induced turbulence promotes larger shear generation due to stronger coupling between the fire and atmosphere. It should

also be recognized that the convection increased the turbulence not only in the vertical and along-wind component, but also in the crosswise direction (Fig. 13a, b) indicating that the three-dimensional fire-induced turbulence may influence fire behaviour over sloping terrain.

4 Conclusions

Fire–atmosphere interactions were measured during a small field experiment conducted on a grass-covered hill in an environment associated with a stable, marine boundary layer and a cross-slope surface flow. This observational study highlights the complex interaction of fire, meteorology, and topography that affects fire behaviour in complex terrain. The fire was ignited using a team of firefighters who started the ignition as a head fire at the bottom of the hill and ending on the upwind edge of the experimental plot. The fire spread quickly through the instrument tower, and the smoke column tilted downwind as a single longitudinal vortex with a clockwise rotation.

Observations from this experiment show that convective heat generated from the fire front is advected downwind close to the surface in the lowest 2 m a.g.l. This near-surface advection dominates the heat transfer to the fuels. Observations also showed that, even for a moderate wind speed of $7\,\mathrm{m\,s^{-1}}$, where the fire front spreads up and across the slope, convective heat fluxes dominated over radiative heat flux for the duration of the fire-front passage except for a short period when radiation was greater just in front of the fire line. This period coincided with downslope flow that advected the plume down the slope briefly. During the fire-front passage, horizontal heat fluxes were nearly equal at the surface and at 12.0 m a.g.l., but at the surface the along-slope directed heat flux was larger indicating that the heat was driven up the slope perpendicular to the fire front. This was most likely due to a fire-induced circulation that formed in response to the ambient shear and thermal instabilities generated by the fire.

A minimum in atmospheric pressure was observed at the fire front with a decrease of 0.4 hPa that coincided with a strong updraft core of nearly $8\,\mathrm{m\,s^{-1}}$. These observations provide evidence that even under moderately windy conditions the pressure minimum associated with the fire remains rather close to the combustion zone. The turbulence associated with the fire-front passage was characterized by more isotropic behaviour at 12.0 m a.g.l., while less isotropic conditions were present at 1.9 m a.g.l. due to higher variance in the horizontal winds at the fire front. The buoyancy production caused by a large increase in the sensible heat flux from the fire had a larger contribution to the turbulence kinetic energy compared to the shear generation during the fire-front passage.

Future fire—atmospheric studies should be aimed at better documenting fire behaviour properties during the fire-front passage, a major limitation to this study. Also, simulations using coupled fire-atmospheric models should be performed to better understand the dynamic mechanisms responsible for the observed thermodynamic and kinematic structures reported from this field experiment. Furthermore, observations from this study may provide a useful dataset for evaluating such models for use in regions of complex terrain where wildland fires are common.

Acknowledgments This research was funded by a Research Joint Venture Agreement between the USDA Forest Service - Northern Research Station and San José State University Research Foundation (#07-JV-11242300-073). The Contra Costa County Fire Department and other agencies involved in the planning and operations of the Wildfire 2010 training drill are acknowledged for accommodating our slope fire experiment. We thank Dennis Burns of the Pleasanton Fire Department for helping organize our research objectives into the burn plan. Tim Walsh and crew from the Marin County Fire Department's Tamalpais Fire Crew are

acknowledged for conducting the ignition. The Bay Area Air Quality Management District is thanked for providing the radar wind profiler data. Allison Charland and Dianne Hall are thanked for their help in the field experiment, and Braniff Davis is thanked for drafting Fig. 1. Finally, the authors thank the anonymous reviewers for their comments, which greatly improved the manuscript.

References

Byram GM (1959) Combustion of forest fuels. In: Davis KP (ed) Forest fire: control and use. McGraw Hill, New York, pp 61–89

Cheney NP, Gould JS, Catchpole WR (1998) Prediction of fire spread in grasslands. Int J Wildland Fire 8:1–13

Clark TL, Jenkins MA, Coen J, Packham D (1996) A coupled atmosphere-fire model: convective feedback on fire-line dynamics. J Clim Appl Meteorol 35:875–901

Clements CB (2011) Effects of complex terrain on extreme fire behaviour. In: Synthesis of knowledge of extreme Fire behaviour: vol I for Fire Managers. U.S. Department of Agriculture, Forest Service, Pacific Northwest Research Station, 144 pp

Clements CB, Zhong S, Goodrick S, Li J, Bian X, Potter BE, Heilman WE, Charney JJ, Perna R, Jang M, Lee D, Patel M, Street S, Aumann G (2007) Observing the dynamics of wildland grass fires: FireFlux—a field validation experiment. Bull Am Meteorol Soc 88:1369–1382

Clements CB, Zhong S, Bian X, Heilman WE, Byun DW (2008) First observations of turbulence generated by grass fires. J Geophys Res 113:22102–22115

Coen JL (2005) Simulation of the Big Elk Fire using coupled atmosphere-fire modeling. Int J Wildland Fire 14:49–59

Coen JL, Cameron M, Michalakes J, Patton EG, Riggan PJ, Yedinak KM (2013) WRF-Fire: coupled weather-wildland fire modeling with the weather research and forecasting model. J Clim Appl Meteorol 52:16–38

Cunningham P (2007) Idealized numerical simulations of the interactions between buoyant plumes and density currents. J Atmos Sci 64:2105–2115

Dupuy J-L, Maréchal J (2011) Slope effect on laboratory fire spread: contribution of radiation and convection to fuel bed preheating. Int J Wildland Fire 20:289–307

Filippi JB, Pialat X, Clements CB (2013) Assessment of FOREFIRE/MESO-NH for wildland fire/atmosphere coupled simulation of the FireFlux experiment. Proc Combust Inst 34:2633–2640

Forethofer JM, Goodrick SL (2011) Review of vortices in wildland fire. J Combust 2011:1–14. doi:10.1155/2011/984363

Kochanski A, Jenkins MA, Krueger S (2009) Flow over a simple hill and its impact on wind speed, variability, and turbulence. In: 8th Symposium on fire and forest meteorology, Kalispell

Kochanski A, Jenkins MA, Sun R, Krueger S, Abedi S, Charney J (2013) The importance of low-level environmental vertical shear to wildfire propagation: proof of concept. J Geophys Res 118:8238–8252

Linn RR, Winterkamp JL, Weise DR, Edminster C (2010) A numerical study of slope and fuel structure effects on coupled wildfire behaviour. Int J Wildland Fire 19:179–201

Mell W, Jenkins MA, Gould J, Cheney P (2007) A physics-based approach to modelling grassland fires. Int J Wildland Fire 16:1–22

Morandini F, Silvani X (2010) Experimental investigation of the physical mechanisms governing the spread of wildfires. Int J Wildland Fire 19:570–582

Moreira GAA, Dos Santos AAC, do Nascimento CAM, Valle RM (2012) Numerical study of the neutral atmospheric boundary layer over complex terrain. Boundary-Layer Meteorol 143:393–407

Pimont F, Dupuy J-L, Linn RR (2012) Coupled slope and wind effects on fire spread with influences of fire size: a numerical study using FIRETEC. Int J Wildland Fire 21:828–842

Potter BE (2012) Atmospheric interactions with wildland fire behaviour—I. Basic surface interactions, vertical profiles and synoptic structures. Int J Wildland Fire 21:779–801

Seto D, Clements CB (2011) Fire whirl evolution observed during a valley wind-sea breeze reversal. J Combust 2011:1–12. doi:10.1155/2011/569475

Seto D, Clements CB, Heilman WE (2013) Turbulence spectra measured during fire-front passage. Agric For Meteorol 169:195–210

Sharples JJ (2009) An overview of mountain meteorological effects relevant to fire behaviour and bushfire risk. Int J Wildland Fire 18:737–754

Sharples JJ, Gill AM, Dold JW (2010) The trench effect and eruptive wildfires: lessons from the King's Cross Underground disaster. In: Proceedings of Australian Fire and Emergency Service Authorities Council 2010 conference, Darwin, Australia. http://www.maths.manchester.ac.uk/~jwd/articles/10-TEaEW.pdf

Stull RB (1988) An introduction to boundary layer meteorology. Kluwer, Boston, 666 pp

Sun R, Krueger SK, Jenkins MA, Zulauf MA, Charney JJ (2009) The importance of fire–atmosphere coupling and boundary layer turbulence to wildfire spread. Int J Wildland Fire 18:50–60
Taylor PA, Teunissen HW (1987) The Askervein Hill project: overview and background data. Boundary-Layer Meteorol 39:15–39
Viegas DX (2002) Fire line rotation as a mechanism for fire spread on a uniform slope. Int J Wildland Fire 11:11–23
Viegas DX (2004) Slope and wind effects on fire propagation. Int J Wildland Fire 13:143–156
Viegas DX (2005) A mathematical model for forest fire blow-up. Combust Sci Technol 177:1–25
Viegas DX, Pita LP (2004) Fire spread in canyons. Int J Wildland Fire 13:253–274
Viegas DX, Simeoni A (2010) Eruptive behaviour of forest fires. Fire Technol 47:303–320
Viegas DX, Cruz MG, Ribeiro LM, Silva AJ, Ollero A (2002) Gestosa fire spread experiments. In: Viegas DX (ed) Proceedings of the IV international conference on Forest fire research and wildland fire safety, Luso, Portugal, 18–23 November 2002. Millpress Science Publishers, Rotterdam
Weise DR, Biging GS (1997) A qualitative comparison of fire spread models incorporating wind and slope effects. For Sci 43:170–180
Werth PA, Potter BE, Clements CB, Finney MA, Goodrick SL, Alexander ME, Cruz MG, Forthofer JA, McAllister SS (2011) Synthesis of knowledge of extreme fire behaviour: vol I for fire managers. U.S. Department of Agriculture, Forest Service, Pacific Northwest Research Station, 144 pp
Whiteman CD (2000) Mountain meteorology: fundamentals and applications. Oxford University Press, New York, 355 pp
Wilczak JM, Oncley SP, Stage SA (2001) Sonic anemometer tilt correction algorithms. Boundary-Layer Meteorol 99:127–150